



Contents lists available at ScienceDirect

# Journal of Wind Engineering and Industrial Aerodynamics

journal homepage: [www.elsevier.com/locate/jweia](http://www.elsevier.com/locate/jweia)

## An observational climatology of anomalous wind events at offshore metemast IJmuiden (North Sea)



Peter C. Kalverla<sup>a,\*</sup>, Gert-Jan Steeneveld<sup>a</sup>, Reinder J. Ronda<sup>b</sup>, Albert A.M. Holtslag<sup>a</sup>

<sup>a</sup> Meteorology and Air Quality Section, Wageningen University, PO box 47, 6700 AA Wageningen, The Netherlands

<sup>b</sup> Royal Netherlands Meteorological Institute, Utrechtseweg 297, 3731 GA De Bilt, The Netherlands

### A B S T R A C T

Uncertainty reduction in offshore wind systems heavily relies on meteorological advances. A detailed characterization of the wind climate at a given site is indispensable for site assessment, and its accurate representation in load assessment models can reduce costs of turbine design and the risk of failure. While regular wind conditions are reasonably described by established methods, some atypical wind conditions are poorly understood and represented, although they contribute substantially to load on turbines. In this study, 4 years of high-quality observations gathered up to 300 m are analyzed to characterize the wind climate at the IJmuiden tower, focusing on these ill-defined conditions. Following a systematic approach, six ‘anomalous wind events’ are identified and described: low-level jets, extreme wind speeds, shear, veer, turbulence and wind ramps. In addition, we identify typical weather conditions that favour their formation. Stable stratification in spring and summer leads to low-level jets (up to 12% of the time) for moderate wind conditions, and to extreme wind shear for stronger wind regimes. Typical wind ramps lead to a change in wind speed of  $2 \text{ m s}^{-1}$  in one hour. The applicability of turbulence intensity as a measure of turbulence and gusts is found to be questionable.

### 1. Introduction

Wind energy has been established as an outstanding resource of renewable energy, with over 433 GW of installed capacity by the end of 2015 worldwide (REN21, 2016). Onshore wind power has now become cost-competitive with traditional sources, and offshore wind power follows this track. Offshore wind farms have the advantages of stronger and steadier winds than onshore, more available space, less visual distortion, and less noise pollution, among others. The worldwide installed offshore wind power was estimated at 12 GW by the end of 2015 (REN21, 2016), with the largest share in Europe with 7.5 GW divided over 76 offshore wind farms (Rodrigues et al., 2015). A further increase to 40 GW is imperative to reach the European Union’s target of 20% renewable energy by 2020 and follow-up targets thereafter (European Wind Energy Association, 2013). Despite recent advances and numerous assets of offshore wind, continued growth is still hampered by relatively high installation and maintenance costs and uncertainties in average wind on short and longer time scales (European Wind Energy Association, 2013; Breton and Moe, 2009; Burton et al., 2011; Rodrigues et al., 2015; Carroll et al., in press; Kuik et al., 2016; Mérigaud and Ringwood, 2016). Maintenance of offshore wind turbines is carried out with large, expensive crane vessels that can

only be put to sea in favourable weather concerning wind and significant wave height. This can lead to long waiting times and extended periods of power loss (Martini et al., 2016). It is thus of utmost importance that turbine failure and maintenance are minimized, which is challenging since the offshore environment is more demanding than its onshore counterpart due to the stronger winds, additional wave and current loads, and corrosion by salty water.

To minimize turbine failure, prototype turbines are extensively tested with simulation software, in which the wind field is ‘translated’ to actual forces on the wind turbine (Burton et al., 2011; Vorpahl et al., 2013). Obviously, the input wind field determines the resulting load assessment, but contemporary guidelines (IEC, 2005, 2009; Burton et al., 2011) still rely on idealized extrapolation methods. Fig. 1a conceptually illustrates this approach. A frequency distribution of wind speed at one height is combined with a wind profile parametrization (e.g. power law, logarithmic wind profile) to obtain a suite of ‘representative’ wind profiles. Subsequently, the estimated loads resulting from these profiles are extrapolated to the turbine lifetime ( $\approx 20$  years) using the frequency distribution. Many authors have argued that these methods cannot adequately capture all variability that is observed in the field (Lange et al., 2004; Gryning et al., 2007; Kettle, 2014; Optis et al., 2014; Nunalee and Basu, 2014). For example, they

\* Corresponding author.

E-mail address: [peter.kalverla@wur.nl](mailto:peter.kalverla@wur.nl) (P.C. Kalverla).

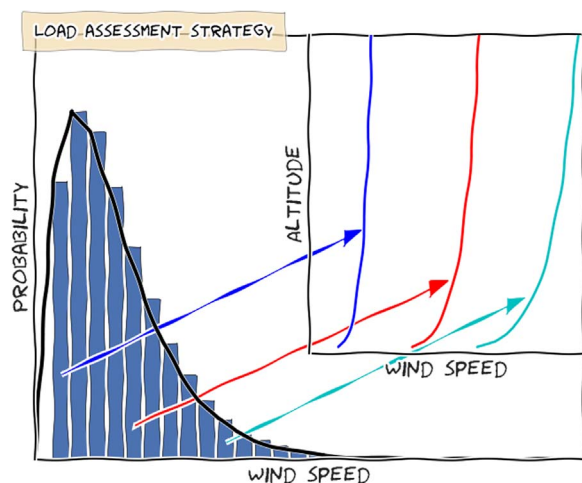


**Fig. 1.** Conceptual figure to illustrate the contemporary guidelines for wind representation. A probability distribution of wind speeds is sampled and for each sample a simple profile parametrization is used to extrapolate the wind speed to other altitudes.

cannot account for atmospheric stability, vertical variations of wind direction, or low-level jets. Therefore, the current methodology leads to substantial uncertainty in the estimated loads.

Apart from the regular wind conditions, the IEC also specifies load cases to account for ultimate loads resulting from extreme wind speeds, extreme gusts, and extreme shear (IEC, 2005; Burton et al., 2011). These wind events are described in a rather idealized fashion, e.g. extreme shear is simulated with a mathematical function that tilts the wind profile with a fixed factor. This approach is physically unrealistic and therefore leads to additional uncertainties in the load estimates. Finally, although the current methodology does account for short-term wind fluctuations, it does not consider temporal transitions in the mean wind profile. In the context of power forecasting, these so-called ‘wind ramps’ have received considerable attention recently (Gallego et al., 2014; Gallego-Castillo et al., 2015; Kiviluoma et al., 2016), but to our knowledge wind ramps in relation to wind farm site or load assessment have not been assessed so far.

Thus, the realism of the wind climate as represented in load assessment studies is open for further improvement, at least for a number of conditions that are currently not- or ill-defined. In this paper, we use a unique observational dataset obtained with a tall tower and lidar observations up to 300 m height, situated 85 km off the Dutch coast, to investigate the wind climate at the North Sea and obtain a reference climatology of these ‘anomalous wind events’ (viz. low-level jets, extreme wind speed, shear, gusts and ramps. Although it would be possible to define more events, such as thunderstorm downbursts and waterspouts, these are very hard to measure and are therefore not part of this study. A useful reference on the latter may be found in Dotzek et al. (2010)). Accordingly, we formulated the following research questions:

1. What are typical values and temporal characteristics of low-level jets, extreme wind speed, shear, gusts and ramps?
2. How are wind, wave and other weather conditions related to these anomalous wind events?
3. Can we identify temporal overlap between the anomalous wind events?

The first question deals with objectively defining each of the anomalous wind events, and is in fact one of the unique aspects of this study, enabling straightforward comparison with other datasets and model validation. The typical conditions of question 2 will help us to characterize the AWEs. An analysis of potential temporal overlap between events is included in order to obtain reliable statistics considering that multiple extremes may occur simultaneously. The resulting climatology of anomalous wind events

characterizes the wind variability at the site, and is particularly well-suited as a reference for future studies. As such, this may serve as a first step towards more accurate description of the anomalous wind events in load assessment studies.

## 2. Background

This section provides a brief overview of each of the identified anomalous wind events.

**Low-level jets.** A low-level jet (LLJ) is a maximum in the vertical wind speed profile, relatively close to the surface (Baas et al., 2009; Nunalee and Basu, 2014). When located in the rotor plane, the increased wind speed might boost the power production, but can also lead to enhanced wind loads on the turbines. E.g. Gutierrez et al. (2016) used high-frequency tower observations up to 200 m and found that the enhanced wind shear during LLJs leads to higher structural loads on turbines. Park et al. (2014) performed a similar study using wind input from large-eddy simulations and found comparable results. Therefore, accurate LLJ representation is critical in atmospheric models and in load assessment models and in site assessment studies. Mirocha et al. (2016) recently evaluated the representation of LLJs in the Weather Research and Forecasting model (Skamarock and Klemp, 2008) and found that “The considerable root mean square error and bias values, even among the ‘best’ performing simulations, underscore the need for improved simulation capabilities for the prediction of near-surface winds during LLJ conditions.”

Several physical mechanisms for the LLJ have been hypothesized (Stull, 1988; Stensrud, 1996). Over land, LLJs can be explained by the evening transition, when turbulent mixing decays (Baas et al., 2009; Van de Wiel et al., 2010). The reduced friction leads to acceleration of the wind at the top of the ‘decoupled’ layer. This jet follows an inertial oscillation with a period equal to the coriolis period at a given latitude (appr. 15 h for the Southern North Sea). A jet formed over land and subsequently advected offshore, may well be able to persist there. Alternatively, a similar mechanism can occur when warm air mass is advected over a cold (sea) surface (Smedman et al., 1989; Dörenkämper et al., 2015). The bottom cooling leads to a stably stratified layer which can also ‘decouple’ from the flow aloft. Other authors have linked low-level jets to baroclinicity and strong horizontal temperature gradients (Zemba and Friehe, 1987; Burk and Thompson, 1996; Andreas et al., 2000). These jets have a direction more or less parallel to the coast (Stensrud, 1996). Finally, downward mixing of higher wind speeds aloft may lead to short-lived jet-like structures.

**Extreme wind speeds.** Extreme wind speeds are often studied in a statistical sense, e.g. turbine load assessment typically considers the estimated 50-year wind extreme (Burton et al., 2011). For class I turbines, the reference 50-year 10 min-averaged wind extreme is set to  $50 \text{ m s}^{-1}$  (IEC, 2005). A comprehensive overview of statistical extreme value theory application to wind speeds is given in Palutikof et al. (1999). An often encountered challenge is that datasets are too short, since extreme value theory typically selects only one event per year. Therefore, Palutikof et al. (1999) discuss several methods to make optimal use of the available data. At the North Sea, wind extremes are always associated with extratropical cyclones. An interesting meteorological treatment of many storm events is given in Lamb and Frydendahl (1991). Recently, Christakos et al. (2016) presented a detailed investigation of cyclone Xaver that passed over the North Sea in December 2013. The Weather Research and Forecasting model (Skamarock and Klemp, 2008) was used to study the wind power density, and was found to perform rather well. Wind speeds exceeded  $25 \text{ m s}^{-1}$  for 30 h during this extreme event. At the same time, wind power generation reached a new record due to the strong winds associated with the cyclone just before and after this peak wind speed.

**Wind shear and veer.** (Vertical) shear is represented by the change of wind with height. Naturally, the flow must adjust to vanishing wind at the bottom boundary, and therefore most shear is

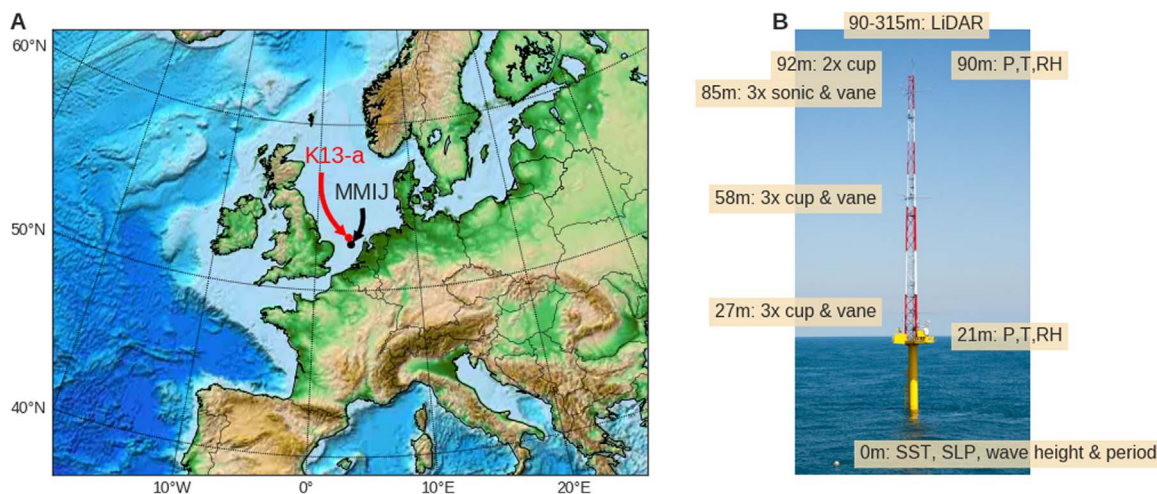


**Fig. 2.** A: Map of northwest Europe, with the location of the IJmuiden meteorological mast and the K13-a oil rig indicated. Source: ETOPO. B: a photograph of the measurement site, with brief annotations explaining the instrumentation.

observed close to the surface, where it can lead to considerable differential loading on wind turbines (Burton et al., 2011). It is thus important to correctly account for wind shear in offshore wind systems.

Shear is sometimes expressed as a ratio of the wind speed between two altitudes. Alternatively, a power-law of the form  $u/u_{ref} = (z/z_{ref})^x$  is sometimes used to describe the relation between wind speed and altitude (Farrugia, 2003; Storm and Basu, 2010). In that case, the exponent  $x$  determines the steepness of the wind profile. In the IEC guidelines  $x$  is fixed at a value of 0.14 for offshore conditions, but in fact  $x$  encompasses information about atmospheric stability and flow characteristics and may thus assume a range of values (Irwin, 1979). Obviously, neither of these methods is applicable to the previously described low-level jets. Additionally, both are unable to represent directional changes.

Since wind is a vector, we can distinguish between velocity shear and directional shear. Velocity shear is the change in wind vector magnitude with height. The change of wind direction with height is called wind veer. Veering with height can occur due to different mechanisms (Brown et al., 2005). Under idealized conditions, Ekman theory predicts 45° wind veering in the atmospheric boundary layer, which in reality reduces to 15–40° depending on stability. Additionally, horizontal temperature gradients lead to a thermal wind that veers (backs) with height if warm (cold) air is advected. The strongest veering is to be expected when the two processes act together. Finally, mesoscale phenomena like the sea breeze may lead to additional rotation of the wind vector with height.

Over 20 years ago, Hollingsworth (1994) already identified serious deficiencies in the ECMWF model representation of backing winds with height during periods of cold air advection. 10 years later, Brown et al. (2005) evaluated the representation of wind turning in the ERA-interim dataset, and found that the model performance is still quite poor, with biases up to 30° under strong baroclinic conditions. They found similar results for higher resolution ECMWF forecasts and for the MetOffice model.

**Turbulence and wind gusts.** Turbulence is an important atmospheric process characterized by chaotic motions on relatively short length and time scales, covering the range between viscous processes on the molecular scale and the mean flow on the scales of the atmospheric boundary layer (Stull, 1988). It is the main driver for transport of heat, moisture and momentum, and as such turbulence governs the environment in which turbines have to operate. This is relevant for wind energy because the rapid motions lead to differential loads on the turbine, and to power fluctuations. Turbulence is responsible for wind gusts that are superimposed on the mean wind. Therefore, studies focusing on wind energy often report the so-called

turbulence intensity, i.e. the standard deviation of the wind speed, normalized by the mean wind speed. Similarly, gust factors can be computed as the ratio of the maximum wind speed to the mean wind. Usually, the gust factor and turbulence intensity are closely related (Bardal and Sætran, 2016).

**Wind ramps.** Wind ramps are rapid changes in the wind speed or direction in time (within one to several hours). In that sense, they are different from the previously discussed AWEs that were all treated as instantaneous profiles. Sudden fluctuations in the wind speed can result in power fluctuations, especially in the case of large wind farms. Therefore, wind ramps have received considerable attention in the field of forecasting lately (Gallego et al., 2014; Gallego-Castillo et al., 2015; Kiviluoma et al., 2016). Sudden changes in wind direction require adjustment of the rotor orientation. Wind ramps can be governed by different mechanisms, e.g. the passage of fronts, formation of thunderstorms due to moist convection, perturbations in stability leading to downward momentum mixing, or the onset of local circulations like a sea breeze. Since these processes act on various time scales and produce wind fluctuations of different magnitude, many different ramp criteria have been defined (see Gallego-Castillo et al., 2015). The time scales range from 5 min to 6 h, and the power fluctuations vary between 10% and 75%, expressed as percentage of the rated power that was considered in each case study. Gallego-Castillo et al. (2015) encourage that further research is conducted to explain ramp occurrence and its representation in numerical weather prediction models. In this context, it is most relevant to report temporal wind variations in our climatology.

### 3. Methodology

#### 3.1. Description of the dataset

The observations for this study have been gathered at the meteorological mast IJmuiden (MMIJ) (Werkhoven and Verhoef, 2012), situated in the North Sea approximately 85 km off the Dutch coast (52°50.89'N, 3°26.12'E, Fig. 2). The water depth at the site is about 28 m. In the four-year period from 2012 to 2015, a 90 m mast has been maintained and equipped with several instruments. On the platform (21 m) and the top of the mast (90 m), standard meteorological quantities pressure, temperature and relative humidity were observed (Vaisala PTB210 and HMP155). At 27 and 58 m, three booms with Thies first class cup anemometers and wind vanes were mounted to the tower. Moreover, three Metek USA-1 sonic anemometers and three more wind vanes were mounted at 85 m. Two additional cup anemometers were mounted at the top of the tower (92 m). A Zephir 300

continuous-wave Lidar recorded wind speed and direction at 25 m intervals between 90 and 315 m. Finally, a Triaxis wave buoy recorded wave and current characteristics, as well as water temperature and sea level pressure. Compared to other masts at the North and Baltic Seas, MMIJ stands out because of its measurement height (up to 315 m), its distance to shore, and because it has three booms at each measurement altitude, allowing for the elimination of mast disturbances. For comparison, the Høvsøre tower (Peña et al., 2015) is located at the coastline and is 116 m tall. In addition, the widely used FINO-1,2,3 towers reach up to a height of 100 m. Moreover, FINO-1 and 2 are situated closer to the coast (40 m) and in the vicinity of wind farms. Therefore MMIJ offers the opportunity to investigate undisturbed wind patterns for higher altitudes than before.

Data postprocessing has been performed by the energy centre of the Netherlands (ECN) before uploading to <http://www.meteomastijmuiden.nl/data/>. All data are provided as 10-min averages, standard deviations, and min/max values, except for the buoy data, which are available at hourly intervals. Care was taken to minimize the effects of tower distortion, using the differences between sensors at the different booms. This procedure is outlined in the instrumentation report (Werkhoven and Verhoef, 2012). Using the one level of overlap between the Lidar and cup-anemometer measurements (90 m), ECN also performed a validation of the Lidar data (Maureira Poveda and Wouters, 2014). Good agreement was found between mean wind speed and direction (mean bias of 1%). However, Lidar-based turbulence intensities appear to be largely overestimated at low wind speeds. Peña et al. (2009) also evaluated a Zephir Lidar against observation from cup anemometers, and conversely, they find an underestimation of turbulence intensity, which they attribute to attenuation of standard deviation observations from the Lidar. They also explain that the Zephir Lidar relies on a thermal wind sensor to determine the sign of the wind direction. This sometimes leads to an 180° error in the wind direction. For the two years of data that were analyzed by ECN, this occurred for 3.6% of the records (Maureira Poveda and Wouters, 2014). Indeed, several instances of this 180° deviation were present in the Lidar data, as well as some spikes in wind speed. These records were carefully removed from the dataset (≈4%).

Several instruments were subject to technical problems during extended periods of time. The wave buoy has been offline between February 2013 and April 2014. In April 2015, most instruments mounted to the mast were disconnected. The 85 m booms did not record from January to mid-August 2013. To obtain wind profiles that are more or less uniformly spaced, we averaged the 85, 90 and 92 m measurements. Performing these adjustments resulted in a data coverage of 84% concerning all wind observations. Considering hub-height wind speed, data availability appears to be 95%, but with fewer measurements in spring. Still, this is a satisfactory data availability for our research purpose, especially considering the remote location of the tower. Because much of the buoy data from MMIJ was missing, we used observations from a nearby oil rig, K13-a, for the classification of waves (see Fig. 2). This station is part of the Dutch network of automated weather stations. Sea state observations from K13-a are publicly available via the Dutch 'Rijkswaterstaat' via <http://www.live.waterbase.nl>. For the episodes with joint data availability, a significant correlation ( $r^2=0.95$ ) was found between K13-a and MMIJ for significant wave height and period. Because of the superior data availability and long standing record, we decided to use K13-a wave data rather than MMIJ observations. Unfortunately, sea surface temperature was not available at K13-a.

Note that Holtslag et al. used one year of the MMIJ dataset (2012) to validate Monin-Obukhov similarity theory for this offshore site (Holtslag et al., 2015) and later to assess wind turbine fatigue loads resulting from the joint probability of stability and wind speed (Holtslag et al., 2016). We extend their work by including all four years of observations, and moreover, we focus on anomalous wind events that are typically not well described by Monin-Obukhov similarity theory.

### 3.2. Definition of anomalous wind events

In this section we objectively define the criteria for the anomalous wind events as introduced in the previous section. To identify low-level jets, the criterion by Baas et al. (2009) is often used nowadays. They define a LLJ as the lowest maximum that is at least  $2 \text{ m s}^{-1}$  and 25% stronger (=20% fall-off) than the subsequent minimum. Earlier studies have used slightly different fall-off criteria, and the choice for any criterion is quite arbitrary. We decided to use Baas' absolute fall-off criterion of  $2 \text{ m s}^{-1}$ , but to perform additional sensitivity analysis of the effects of using a  $0.5 \text{ m s}^{-1}$  higher and lower threshold.

To quantify extreme wind speed, we first apply statistical extreme value analysis to the 115 m wind speed, which corresponds to the hub height of the Leanwind 8 MW reference wind turbine (Desmond et al., 2016). As the dataset is rather short for such a procedure, we apply the method of independent storms, as outlined in Palutikof et al. (1999). In this approach, independent storms are separated by periods of low winds (so-called lulls). This guarantees independence of the data, while at the same time allowing for several extreme events per year. The wind speed maxima  $x$  of the independent storms are then sampled, sorted, and plotting positions are calculated according to

$$F(x_m) = \frac{m - 0.44}{N + 12} \quad (1)$$

where  $m$  is the sorted index and  $N$  is the total number of events. Following Harris (1999), we can then calculate the (Gumbel) reduced variate as

$$y = -\ln(-r \ln(F(x_m))) \quad (2)$$

where  $r$  is the average amount of storms per year. Cook (1985) found that a reliable estimate of the 50-year wind extreme is made for  $r=10$ , leading us to define a lull threshold of  $21.3 \text{ m s}^{-1}$ . To calculate the standard error of the estimate, we used a Monte Carlo method in which we repeatedly drew random samples from the extreme value distribution defined by the parameters that we first identified. Subsequently, these samples were fed back to the extreme value algorithm to obtain a realistic range of values for the two parameters.

For analyzing wind shear and veer, we assume that the turbine always aligns the rotor axis with the mean wind speed at hub height. Accordingly, we can split the wind measurements, and thus the shear, in streamwise and normal components, the latter resulting from changes in wind direction. Note that it is not possible to directly convert between veering angle and normal wind shear, since the same wind shear vector will have a different veering angle for different wind speeds. We prefer this method, in which we express the directional shear in a normal wind component rather than an angle, because in this way the amount of shear can be compared without considering the absolute wind speed, and moreover, because it is more readily translated to forces on the turbine. Fig. 3 clearly illustrates that for a veering wind profile, the normal wind component is positive below hub height and negative above, which seems consistent with the clockwise rotation of the rotor. Because the vertical extent of MMIJ is not a universal property, we will calculate and report the accumulated shear in 6 layers of equal depth (50 m) as

$$S_s = \frac{1}{50} \sum_{z=1}^{50} |s_z - s_{z-1}| \Delta z \quad (3)$$

$$S_n = \frac{1}{50} \sum_{z=1}^{50} |n_z - n_{z-1}| \Delta z \quad (4)$$

where  $s$  and  $n$  denote the streamwise and normal components of the wind vector, respectively. Because the boundaries of these 6 layers do not coincide with the observation heights, we linearly interpolated between the wind observations (assuming that the wind vanishes at the surface). This appeared to be the best method, considering that for

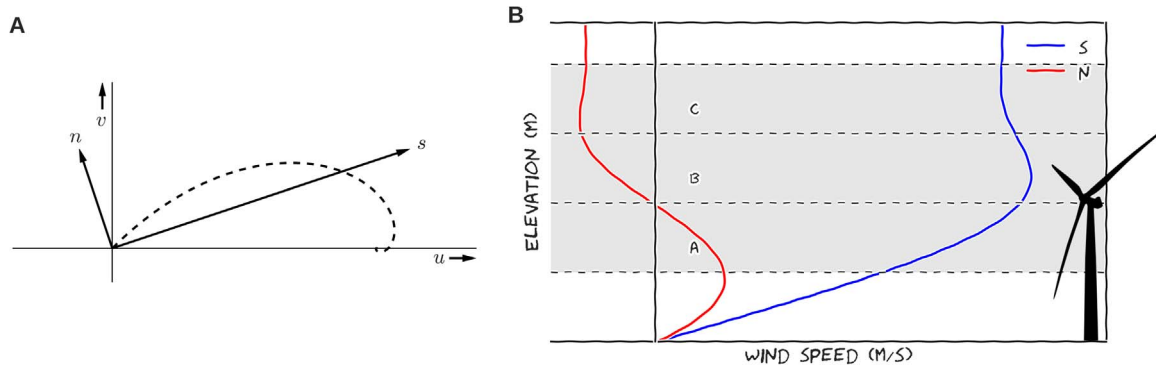


**Fig. 3.** A. Hodograph of a typical Ekman wind profile that veers with height in the boundary layer. The rotated coordinate system is defined by *s*, aligned with the wind at hub height and *n*, perpendicular to *s* and positive to the left. B. Typical vertical profiles of the rotated wind components. The shading represents three layers spanning most of the rotor plane (see Section 3).

most wind profiles, the layer where a logarithmic wind profile would be appropriate was below the lowest measurement height. Additionally, a logarithmic wind profile is not suitable for anomalous events like LLJs. Using polynomial interpolation we found that more artefacts were introduced than realism gained. Taking the magnitude of the vertical differences in *s* and *n* in (3) ensures that ‘negative shear’ is also accumulated. This is relevant, because otherwise the accumulated shear might equal zero if a low-level jet would occur in the middle of a layer, for example. To the authors’ best knowledge this approach has not been reported elsewhere so far.

For the classification of extreme turbulence and associated wind gusts, we use the turbulence intensity,  $TI = \sigma_v/\bar{v}$ , as is common practice in the wind energy sector. In a preliminary study we found a very strong relation between TI and gust factor, similar to Wieringa (1973) and Burton et al. (2011). Therefore, and in the absence of higher frequency data that would provide us with more specific information on gusts, we decided to focus only on levels of turbulence as a proxy for wind gusts. Because the Lidar values of the variance are not very reliable, we only use the data from the cup anemometers and the sonic. To investigate the impact of dividing by the mean wind speed in the definition of TI, we will also discuss the results if only the standard deviation of the wind,  $\sigma_w$ , would be used.

Previous studies that focused on identifying (power) ramps used thresholds ranging from 10% to 75% of the rated power of a wind farm that should be exceeded within a specified time frame of 5 min to 6 h (Gallego-Castillo et al., 2015). Note that these studies used time series of produced wind power rather than time series of wind speed itself, because their focus was on evaluating power forecasts. The diversity in ramp definitions demonstrates that there is no general consensus on the relevance of certain power fluctuations. Alternatively, we focus on fluctuations of the wind itself. Additionally, we do not choose arbitrary fixed thresholds, because in the context of a climatological paper, it makes more sense to convert the criterion again. We evaluate the difference between two consecutive wind profiles and analyse the 5- and 95-percentiles. This yields the 10-min ramp for each observation height. We take the maximum ramp for each record and use the 95-percentile as threshold for classification as extreme ramp event. Similarly, we define the 30-min and 60-min ramps by taking the difference between observations separated by 30 and 60 min of time, respectively. We perform the analysis for both wind speed and direction.

### 3.3. Weather conditions

Having defined all anomalous wind events, our objective is to assess their temporal variability and to relate them to other weather variables. This is important to help us understand the mechanisms that control these events. Additionally, if it is possible to relate anomalous wind events to typical weather patterns, this provides very valuable information, for example in forecasting, where the exact manifestation of

anomalous wind events may not be predicted, but can be estimated based on other (better represented or larger scale) parameters. Likewise, it may provide a starting point for ‘smart sampling’ methods, where one wants to represent most of the variability with as few as possible simulations.

The analysis pointed out that the following five variables (in addition to seasonality) provide valuable information about the typical conditions for each AWE: wind direction, mean wind speed, pressure, stability and wave characteristics. The other parameters in the dataset added little value to the analysis and are therefore not discussed. We use the pressure observed at 21 m because data availability is higher than for sea-level pressure that was measured with the wave buoy. Stability is determined by evaluating the bulk Richardson number between the tower top and the platform:

$$Ri_B = \frac{\frac{g}{\theta_v} \frac{\Delta\theta_v}{\Delta z_\theta}}{\left(\frac{\Delta u}{\Delta z_u}\right)^2 + \left(\frac{\Delta v}{\Delta z_v}\right)^2} \quad (5)$$

where *g* is the gravitational constant, and  $\theta_v$  is the virtual potential temperature. The sign of  $Ri_B$  depends on the density stratification: if density increases with height (virtual potential temperature decreases), the buoyancy term (numerator) is negative and the atmosphere is said to be unstably stratified, and turbulence will be enhanced. If the density decreases with height,  $Ri_B$  is positive and turbulence is suppressed by buoyancy. The shear term (denominator) is by definition positive as it will always lead to dissipative mixing. If  $Ri_B$  is close to zero, the atmosphere is said to be neutrally stratified. We refrain from defining a range of neutral stability, because this bulk layer is relatively thick and elevated, and typical surface layer characteristics are hence not applicable. It would also be possible to evaluate  $Ri_B$  between the platform and the sea surface, which may be more appropriate to reflect surface layer properties. Unfortunately, missing buoy data prevented us to do so for many relevant records. However, for the period where both layers are available, we find that they agree very well. Additionally, we estimated the Obukhov length *L* by an iterative procedure explained in Van Wijk et al. (1990). The results were qualitatively similar to the climatology of the bulk Richardson number, but we prefer the latter because Monin-Obukhov similarity theory is only valid in the surface-layer (which can be very shallow offshore), and moreover, because we are especially interested in the conditions for which this theory is not applicable (e.g. low-level jets).

The wave characteristics will be summarized in the Charnock parameter as defined by Donkers et al. (2011):

$$\alpha = \frac{H}{T\sqrt{gd}} \quad (6)$$

where *H* is the wave height, *T* is the wave period, *g* is the gravitational

constant and  $d$  is the water depth. The parameter thus encompasses information about wave height as well as wave steepness. The value of the Charnock parameter represents the strength of the coupling relation between wind profile shape and wave height. As such, it is used to correct the logarithmic wind profile for roughness over sea. A high value of the Charnock parameter implies a strong coupling, i.e. a direct interaction or equilibrium between wind and waves. Lower values indicate that the wave field is dominated by older waves or swell, and accordingly the surface is smoother.

To analyse the anomalous winds in relation to these conditions, we will consider a batch of relevant events and classify them in a boolean framework. For LLJs this is straightforward, as we used a fixed threshold which must be exceeded. Having no physical considerations at hand that lead to a natural choice of threshold values, we used a different criterion for all other AWEs. Instead of analyzing how often a certain threshold is exceeded, we will report the threshold that is exceeded exactly 5% of the time (i.e. the 95-percentile). This threshold yields a suitable balance between the ‘extremeness’ of the events, and the amount of observations needed for a climatological analysis. For extreme wind speed, we will find exactly 12 quantile values, one for each altitude. However, for our boolean framework we need a criterion that allows us to classify the entire wind profile as one extreme wind event, rather than identifying extreme events for each measurement height. Therefore, we will use the maximum wind speed in each record. For wind shear and veer, we will use the three layers (50–200) that span most of the rotor plane of a current-day wind turbine. We exclude the lower layer as it would dominate the complete climatology. For turbulence we take the maximum of the profile, and for wind ramps we use the 115 m wind as it is close to the hub height of current-day wind turbines.

The relation between the occurrence of each AWE and each of the external conditions was studied by dividing the external condition into bins and counting the number of AWEs in each bin. In an absolute sense, these counts often resemble the distribution of the underlying external condition. In relative sense, i.e. the counts of AWEs for each bin divided by the total number of observations in that bin, some distinctive patterns are revealed (see Section 4).

## 4. Results

### 4.1. Background meteorological conditions

Before we proceed with the classification of anomalous wind events, it is important to understand the meteorological background on which the AWE climatology is projected. The mean wind speed at hub height (115 m) over all seasons amounts to  $10.2 \text{ m s}^{-1}$ . The 2-parameter Weibull distribution, that was fitted to the data using a maximum likelihood function, provides a reasonable fit to the measurements (Fig. 4A). Its shape and scale parameters amount to 2.17 [-] and  $11.49 \text{ m s}^{-1}$ , respectively. The wind climate is dominated by the frequent passage of mid-latitude cyclones, resulting in relatively strong winds from the southwest (Fig. 4B). The mean wind profile, obtained by time-averaging of the wind speed observations at all altitudes demonstrates that most wind shear is confined to the lowest layer, even below the lowest observation height (Fig. 4C). In winter, the mean wind profile is about  $5 \text{ m s}^{-1}$  stronger than in summer and more wind shear is present in the rotor layer of the wind turbines. The figure also illustrates Weibull-weighted mean wind profiles obtained by extrapolation of the 115 m wind using the power law  $u/u_{ref} = (z/z_{ref})^x$  (with fixed exponent of  $x = 0.14$ ) and a neutral logarithmic wind profile  $u = u_{ref} \ln(z/z_0) / \ln(z_{ref}/z_0)$  with  $z_0 = 0.0002 \text{ m}$  (see Holtslag (1984), Foken (2006) and Burton et al. (2011)). A few points were added in the lowest layer to compare the behaviour of the two surface-layer parametrizations. It appears that the power law overestimates the amount of wind shear throughout the wind profile. The logarithmic wind profile performs better.

The bulk Richardson number is positive for 41% of the available observations, and negative for the remaining 59%, i.e. a 2:3 ratio

(Fig. 4D). Even though more observations are missing in spring relative to other seasons, this appears to be a robust figure. If we first calculate monthly means (as such ruling out seasonal variability in the average), the total time fraction of stable and unstable conditions remains nearly unchanged. The magnitude of  $Ri_B$  is inversely proportional to the bulk wind shear, which leads to high absolute values during calm conditions. For the unstable regime, the magnitude of  $Ri_B$  is somewhat higher because the boundary layer is typically well-mixed and hence there is less wind shear than under stable conditions.

Stability over the North Sea has previously been studied by Van Wijk et al. (1990) and Coelingh et al. (1992,1996). They used seawater temperature observations from ships, and wind and air temperature observations from various stations, among which also the K13-a oil rig. They estimated the Obukhov length (see Van Wijk et al., 1990), and found predominantly unstable conditions (48–64% versus 23–36% stable). Additionally, a range of neutral stability was identified. As already mentioned, we refrained from defining a range of neutral stability profiles for  $Ri_B$ , since the thresholds would be too arbitrary. However, the distribution of  $Ri_B$  (absolute values are higher on the unstable side of the figure) indicates that more stable than unstable profiles would be classified as neutral. Hence our findings correspond quite well to previous results. This provides confidence that  $Ri_B$  in the 21–90 m bulk layer is a suitable proxy for stability.

$Ri_B$  exhibits a pronounced annual cycle with more stable conditions in spring and summer and unstable conditions in autumn and winter (Fig. 4E). Spring and summer are characterized by an evident diurnal cycle, with more neutral conditions in the afternoon. In September afternoons the Richardson number is substantially lower than the rest of the day, while in winter the diurnal patterns is nearly absent. The seasonal cycle can be related to sea surface temperature, which drops to  $7 \text{ }^\circ\text{C}$  in spring leading to cooling at the bottom boundary and increases to  $17 \text{ }^\circ\text{C}$  in autumn. In contrast, there is no straightforward explanation as to why we observe a diurnal cycle, since the thermal inertia of the sea is too large to follow the diurnal cycle of solar radiation. A plausible explanation seems to be the advection of onshore boundary-layer structures. Dörenkämper et al. (2015) have shown that coastal structures can still be observed over 100 km off the coast under stable conditions, because of limited vertical mixing.

The observed Charnock parameter varies around a mean values of 0.017 (Fig. 4F), with higher values in winter than in summer, but no clear diurnal variability (not shown). This value is quite high compared to previous studies (e.g. Garratt, 1977; Fairall et al., 2003), but within the range reported by Smith (1988). Oost et al. (2001) studied the Charnock parameter for a near-coastal site in the North Sea, and estimating from their Fig. 1, they find an average value of 0.018 ( $=\ln(-4)$ ). In our study, the Charnock parameter has a high linear correlation (0.87) with the 115 m wind speed. This indicates that for stronger winds, the wave field is mostly ‘wind-dominated’, whereas for smaller wind speeds, swell is relatively more important.

### 4.2. Characterization of anomalous wind events

Low-level jets for which the fall-off exceeds  $2 \text{ m s}^{-1}$  are observed 4.6% of the time, but this figure changes to 6.9 or 3.1% when the threshold is increased or decreased by  $0.5 \text{ m s}^{-1}$ , respectively. It is noteworthy that most LLJs are observed at or around 100 m altitude, i.e. exactly in the rotor plane (not shown). This is lower than onshore, where they are typically observed around 250 m (Baas et al., 2009), and underpins their importance for offshore energy purposes. Kettle (2014) already found similar characteristics for the FINO-1 tower in the German Bight, but because of the mast’s limited height, he was unable to identify the full spectrum of jets.

LLJs occur mostly in spring and summer (Fig. 5A). Their temporal distribution closely follows that of stability (compare Figs. 4D and 5A). In an absolute sense, there are approximately as many jets from the NNE as from the SW, but since the southwesterly winds are more

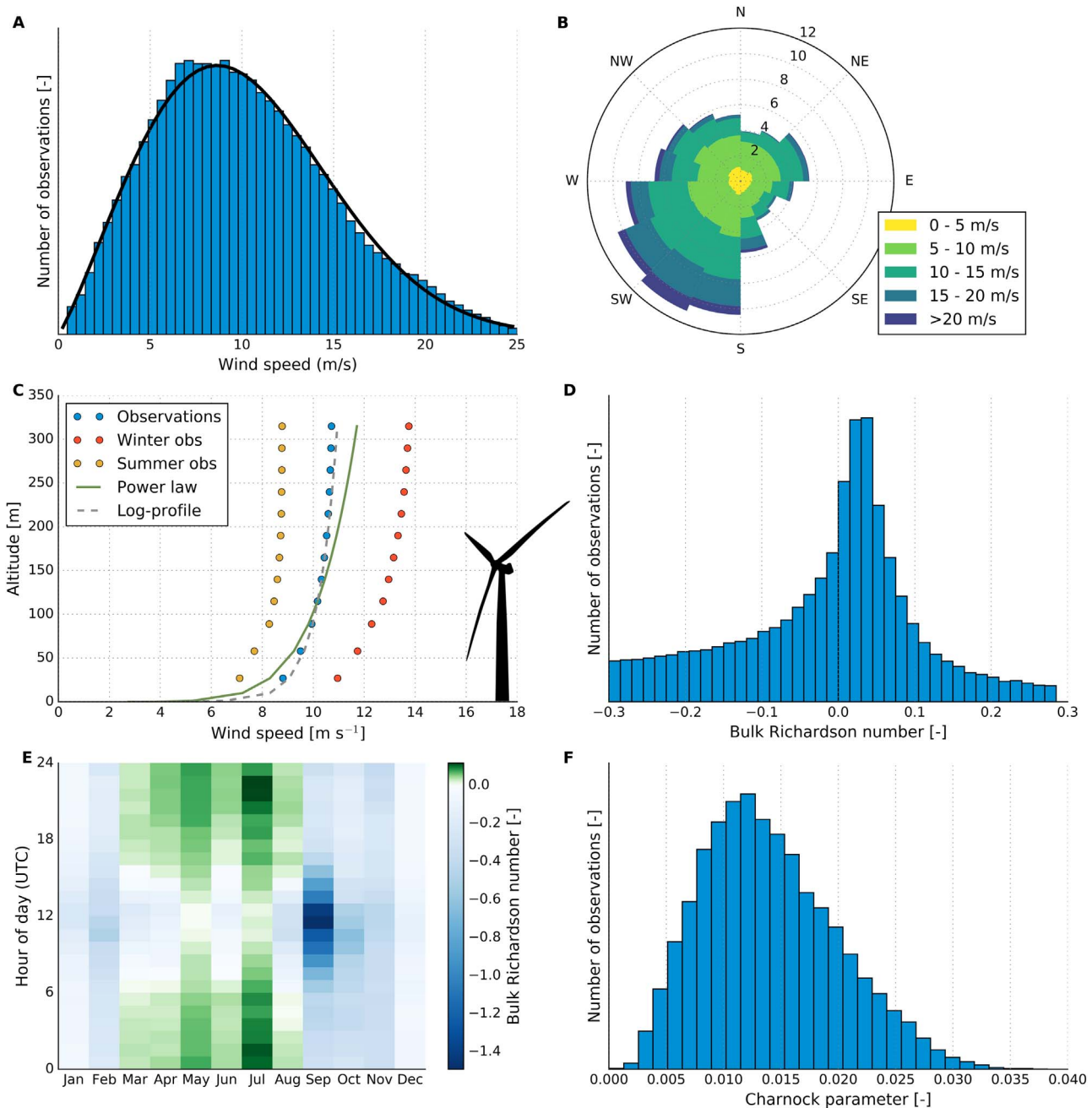


**Fig. 4.** A: 2-parameter Weibull fit to the 115 m wind speed frequency distribution. B: Wind rose of 115 m wind speed and direction in the boundary layer. C: mean wind profile from observations, and by using two weibull weighed extrapolation methods (see text). D: Histogram of  $Ri_{bs}$  evaluated between the top of the mast and the platform. The range was limited to 0.6. E: Median of bulk Richardson numbers grouped by hour of day and month of year. The colourmap was constructed such, that positive values are green and negative values are blue, and their gradients are optimized for their respective ranges. F: Histogram representing the distribution of the Charnock parameter. (For interpretation of the references to color in this figure legend, the reader is referred to the web version of this article.)

abundant in the total dataset, the relative occurrence of LLJs is highest for north-northeasterly winds (Fig. 6B). Jets mostly occur in episodes of relatively high pressure and moderate winds, but some were observed during very low pressure (Fig. 6C). LLJs are usually associated with low values of the Charnock parameter, pointing to low wind-wave coupling or ‘decoupled’ conditions (Fig. 6F). In the light of these characteristics, it seems that multiple mechanisms can lead to wind profiles that are classified as LLJs. Most characteristics support the hypothesis that LLJs form under relatively calm, high pressure situations, when warm continental (NNE) air is advected over a cold ocean (spring/summer) leading to stable stratification ( $Ri_b > 0$ ) and decoupling of the surface layer (low Charnock parameter). Other jets, associated with somewhat stronger southwesterly winds and low-

pressure situations may be related to the passage of fronts or squall lines. This is potentially much more damaging but needs to be further investigated. There are few observations that support the baroclinicity mechanism, since the jet direction would be parallel to the horizontal temperature gradient in that case, which would be a meridional wind in the case of the Southern North Sea.

The hub-height 50-year wind extreme is estimated at  $42.7 \pm 2.4 m s^{-1}$  (Fig. 5B). This is evidently lower than that specified in the IEC guidelines for a class I turbine (reference mean wind speed at hub height =  $50 m s^{-1}$ ). The wind extreme decreases near the surface, but remains more or less constant with height above the tower. Assuming that for strong wind conditions the atmosphere can be described by a neutral logarithmic wind profile, and that there is a strong interaction

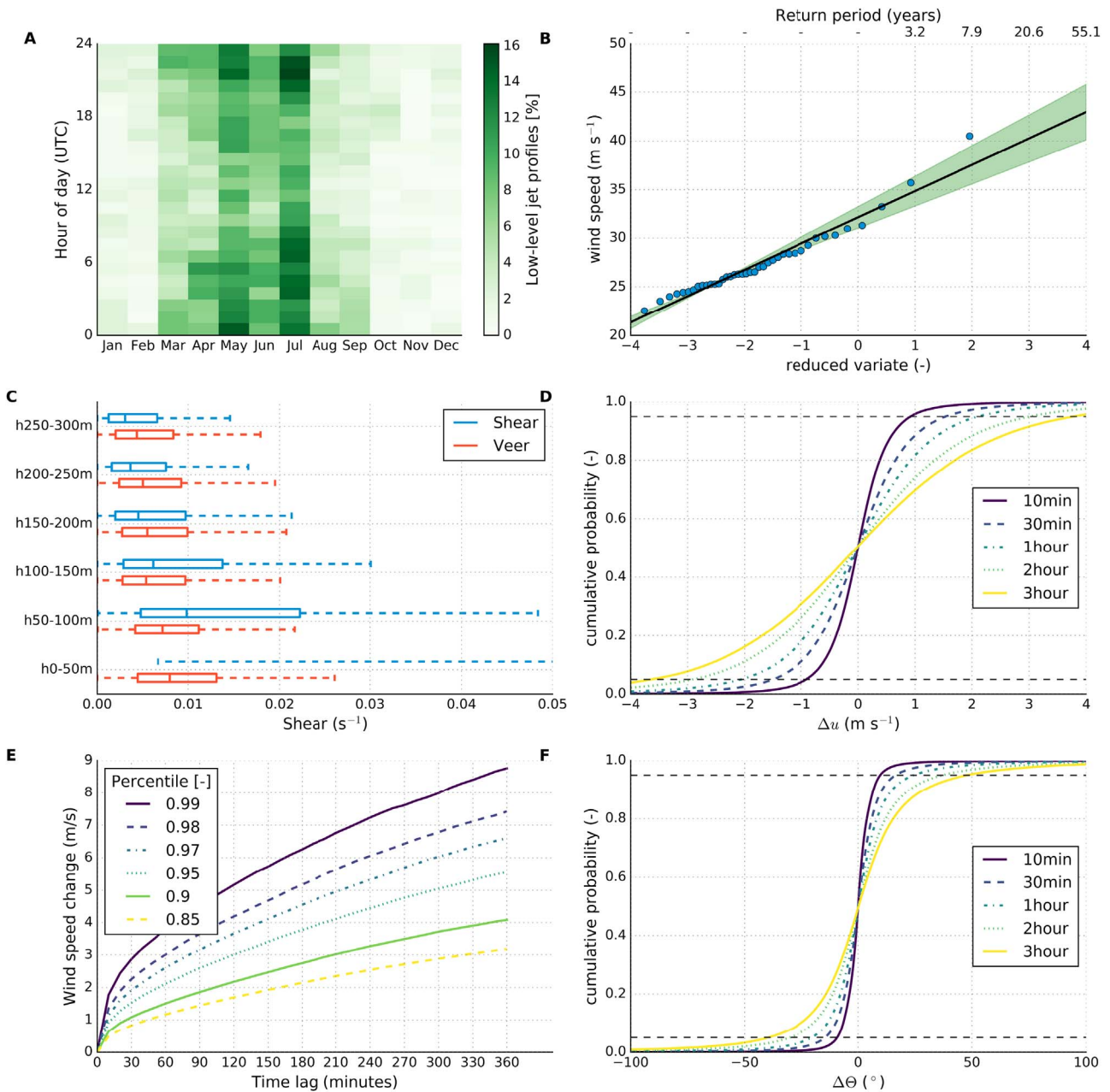


**Fig. 5.** A: Temporal distribution of low-level jet profiles. B: Gumbel plot for extreme value analysis. Return times are indicated on the upper x-axis. C: Boxplots for wind shear and veer distribution over six layers of equal depth. D: Cumulative probability of wind ramps on various time scales. The 5- and 95-percentiles are indicated with dotted horizontal lines. E: Wind ramp magnitude versus time lag for different cumulative probabilities. F: Cumulative probability for wind direction ramps.

between wind and waves (see Section 4.1), we find that the following expression

$$u(z) = \frac{u_*}{\kappa} \ln \left( \frac{gz}{\alpha u_*^2} \right) \tag{7}$$

with  $u_*$  the friction velocity,  $\kappa = 0.4$  the von Karman constant,  $g = 9.81 \text{ m s}^{-2}$  the gravitational constant and  $\alpha$  the Charnock parameter (for which we take a high value of 0.035, consistent with high wind speed observations) provides a reasonable fit to our extreme wind profile with  $u_* = 1.7 \text{ m s}^{-1}$ .

The 95-percentile of wind speed increases with observation height and is around  $19 \text{ m s}^{-1}$  at hub height (115 m). Recall that we focus on this 95-percentile because we want to derive general characteristics of the episodes with the highest winds. Using higher quantiles, some generality might be lost because of insufficient data for a representative sample. Extreme wind speeds usually have a southeasterly direction

and are predominantly observed under low-pressure situations in winter months. These characteristics support the hypothesis that the strongest winds are associated with low-pressure systems. The Richardson number is always near-neutral in these conditions because the lower atmosphere is typically well-mixed due to the strong wind-induced turbulence. Also, there is a strong interaction between wind and waves, characterized by a large value of the Charnock parameter.

The strongest shear is confined to the lowest layer (Fig. 5C). Above 150 m, the normal shear component may become larger than the streamwise shear. 70% of the wind profiles veers with height (not shown), and on average, these profiles have a larger normal component than the other 30% of the data. This may be compensated by the fact that rotor blades are moving along with the normal wind component in veering conditions, whereas they rotate opposite to the normal wind in backing conditions.

Over the rotor plane, the 95-percentile of the streamwise shear

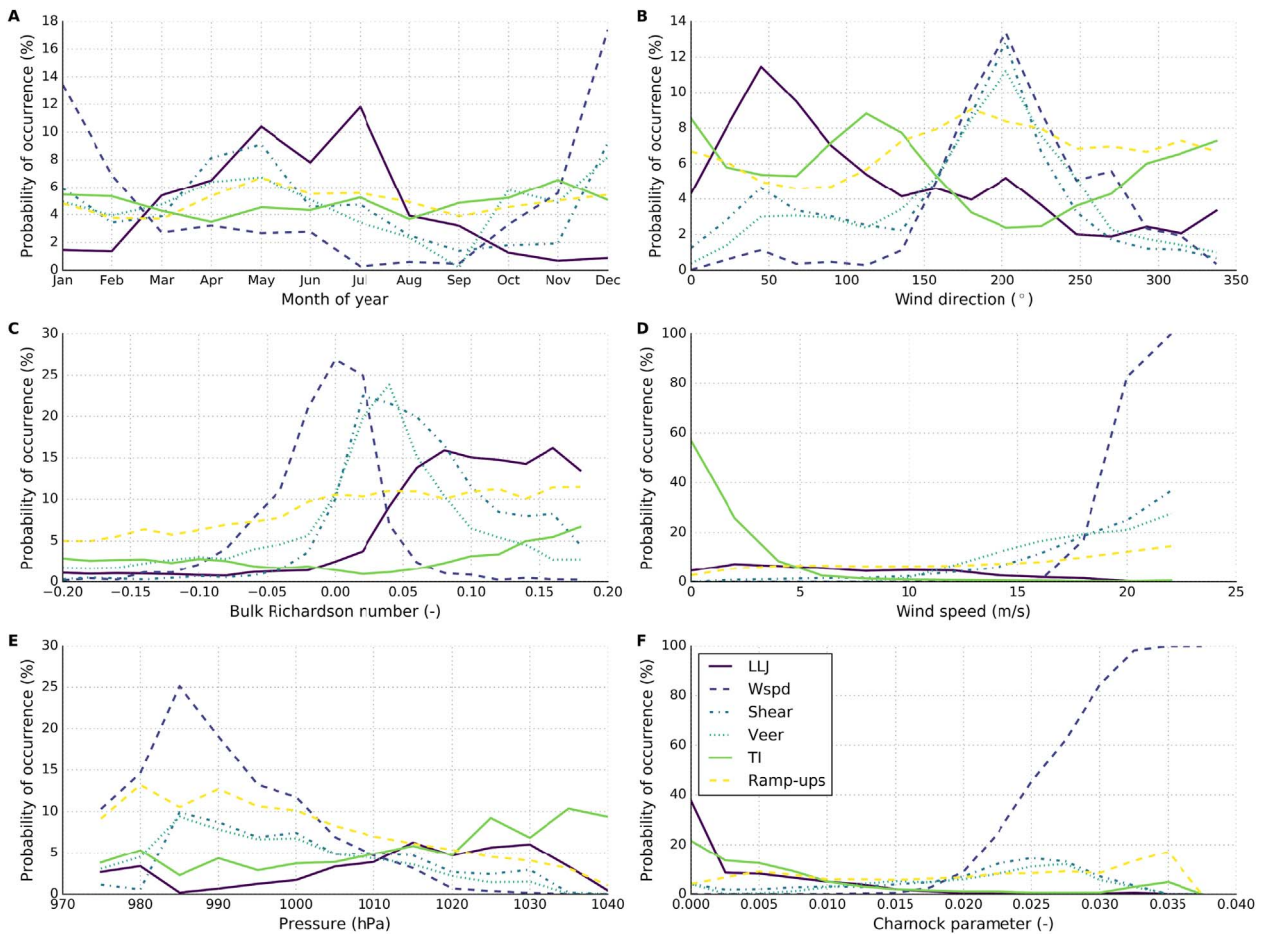


Fig. 6. The relative occurrence of AWEs given A: month of year, B: wind direction, C: stability, D: wind speed, E: pressure, F: Charnock parameter.

amounts to  $0.032 \text{ s}^{-1}$ . Over a 150 m layer, this constitutes a change of  $4.8 \text{ m s}^{-1}$ . Extreme shear is often observed under southwesterly and, to a lesser extent, northeasterly winds (Fig. 6). It peaks in April/May and December/January and is usually associated with a slightly stable stratification. The probability of extreme shear is higher under stronger winds and lower pressure. The Charnock parameter is typically quite high ( $>0.03$ ), although some extreme shear was also observed for very low Charnock parameters. From this climatology we infer that extreme shear is mostly associated with strong SW winds and stable stratification. To understand this, we first note that the absolute value of the Richardson number is by definition small for strong shear. However, as extreme shear is observed more frequently for positive (stable) Richardson numbers than for negative values, it appears that the turbulence-suppressing buoyancy effects allow the stratification to be maintained even under high shear conditions. Conversely, for unstable conditions buoyancy acts to enhance the turbulent mixing and hence the wind speed gradient is smeared out. Additionally, the conditions with NE winds leading to LLJs seems to be favourable for extreme shear as well, although we cannot (yet) conclude whether this shear is indeed associated with low-level jets. This will be further explored in Section 4.3.

The 95-percentile of veer over the rotor plane amounts to  $0.017 \text{ s}^{-1}$ , adding up to  $2.6 \text{ m s}^{-1}$  difference between the top and bottom of the rotor. Inspection of these extreme veer profiles demonstrated that, although veering with height is usually much stronger than backing with height, both cases contribute to the extreme conditions. The climatology of extreme wind veer is quite similar to extreme shear, although the annual cycle is even less distinctive (Fig. 6A). The fact that most veer is observed in stable conditions is in accordance with Van Ulden and Holtslag (1985).

Fig. 6 shows the temporal distribution of turbulence intensity, and

its relation to external variables. Most notably, it appears that TI is highest for (very) low wind speeds, which is a direct result of the fact that TI is by definition inversely proportional to mean wind speed. Essentially, the other figures are just a reflection of this feature. The 95-percentile of TI amounts to 0.13, and the extremes occur under northerly or southeasterly winds, and somewhat more in autumn and winter. Since wind speeds are low, the Richardson number is typically far from neutral. It is predominantly negative (which is consistent with the seasonality, i.e. unstable conditions in autumn and winter), although high values of TI are also observed under stable conditions, as long as the winds are weak. High TI is abundant for high pressure situations and the Charnock parameter is typically low. If, for a brief moment, we put aside our focus on extremes, we can compare the TI climatology with previous work. Hansen et al. (2012) evaluated turbulence intensity for a coastal site in Denmark and found that turbulence is highest for low wind speeds and unstable conditions. This is in line with the findings of Westerhellweg et al. (2011), who analyzed the characteristics of TI as observed at the different FINO towers and with Kettle (2014), who focused on FINO1. It is thus not surprising that we find the extremes for these low wind, unstable conditions. But although our findings make sense from a physical perspective, it is questionable whether these situations with extreme turbulence intensity are indeed the most penalizing conditions for wind turbines. Therefore, we also analyzed the climatology of extreme standard deviations of the winds. The result is exactly opposite, i.e. the largest standard deviations are found under the strongest winds and the climatology now resembles that of extreme mean wind speeds. The 95-percentile of  $\sigma_u$  amounts to  $1.30 \text{ m s}^{-1}$  and high  $\sigma_u$  typically occurs in winter under strong southwesterly winds. With different proxies leading to different climatologies, we are left to conclude that based

on the 10-min means, we cannot identify typical conditions for extreme turbulence and wind gusts in a similar manner as the previously discussed AWEs.

The cumulative probability of wind speed ramp events on different timescales is given in Fig. 5D. A typical 10-min ramp-up event (95-percentile) appears to be characterized by a wind speed change of  $0.9 \text{ m s}^{-1}$ . The ramp distribution appears to be very symmetric, such that typical ramp-downs (the 5-percentile) are of comparable magnitude as the ramp-ups. Organizing the percentile values against time frames summarizes the expected wind ramps (Fig. E), which can be used as a reference for future wind climatologies and ramp studies. The ramp magnitude turns out to be well-described by a square function of the form  $y = a\sqrt{x}$ , with  $a=(1.5, 1.2, 1.1, 0.9, 0.7, 0.5)$  for percentiles (0.99, 0.98, 0.97, 0.95, 0.9, 0.85). Although changes in the order of  $1\text{--}2 \text{ m s}^{-1}$  seem rather minimal, the actual power production is proportional to the wind speed cubed. For the LEANWIND reference wind turbine (Desmond et al., 2016) with a rated power of 8 MW at a wind speed of  $12.5 \text{ m s}^{-1}$ , a typical 1-h ramp at MMJ of  $2 \text{ m s}^{-1}$  (from  $12.5$  to  $10.5 \text{ m s}^{-1}$ ) leads to power reduction of 25% of the rated power, which is a serious ramp event (Truewind, 2008; Gallego-Castillo et al., 2015). However, if a similar ramp occurred at a wind speed well above the rated power, the power would not decrease at all. From this, it is apparent that the actual ramp impact is dependent on the wind speed at which it occurs. Therefore, Fig. 7 shows the typical ramps that can be expected, given a certain wind speed and time lag. Different rows give 3 different probabilities. Not surprisingly, strong ramp-downs are more probable for very high wind speeds and vice versa. The range between 5 and  $20 \text{ m s}^{-1}$  is most relevant for most contemporary wind turbines. Especially the 1-percentile plot for extreme ramp-downs is important, because for this ramp probability the wind speed change is very much dependent on wind speed, as can be seen from the sloping contour lines.

There is no clear seasonality for wind ramps (Fig. 6). Ramp-downs exhibit a slight preference for southwesterly winds, while ramp-ups are equally probable for any wind direction except for easterly winds, for which they occur somewhat less. The strongest ramps are typically observed under relatively strong winds and low pressure, although some are also observed at lower wind speeds. Ramps are slightly more frequent if for  $Ri_B > 0$ . Unfortunately, this climatology does not reveal important clues as to the governing mechanisms for wind ramps.

For changes in wind direction (Fig. 6F), the 95-percentile amounts to 10, 17, 26, and  $54^\circ$  for time shifts of 10, 30, 60 and 180 min, respectively. However, this distribution is asymmetric, and the probability of directional ramps backing in time is a bit smaller; the 5-percentile amounts to 9, 15, 23, 36, and  $48^\circ$ , for the same times shifts, respectively. Large directional ramps are more probable for northerly and southeasterly winds (not shown), but more importantly, the largest directional changes occur under very weak wind conditions and are therefore probably not relevant. Fig. 8 shows the expected directional changes with specified probability, given a wind speed and time lag. Under stronger wind speeds, wind veering is more probable than wind backing in time. A plausible mechanism associated with these ramps is the passage of cold fronts (Wallace and Hobbs, 2006). The fact that strong direction ramps are more probable for northerly and southeasterly winds, in combination with the notion that the strongest shifts occur under weak winds, suggests that these shifts are related to local circulations in the absence of strong synoptic forces, such as the sea breeze (Zack, 2007).

#### 4.3. (In)dependence of wind events

We have seen that the conditions for which various anomalous wind events occur are sometimes similar, and it is possible that they overlap in time, e.g. strong shear might be associated with low-level jets. Therefore, we

analyse in this section the interrelation between the various wind events.

We study the overlap of events using Venn diagrams representing the 95-percentiles of each time series (Fig. 9). Diagram A illustrates that, although part of the LLJs is associated with extreme shear, still most extremes are independent. Likewise, there is some relation between extreme shear and extreme veer, but they do not always coincide. Even though LLJs are typically characterized by changes in wind direction (Baas et al., 2009), the dependence between LLJs and wind veering is only small. In our analysis the veer is expressed as normal wind component that scales with the magnitude of the wind. Therefore, most veer is related to strong winds, whereas LLJs typically occur under moderate winds. The amount of shear averaged over all low-level jet profiles is  $0.025 \text{ s}^{-1}$  over the layer 50–150 m, which is indeed lower than the extreme shear profiles.

Diagram B illustrates that extreme shear and veer regularly coincide with extreme wind speeds. Stability may explain why approximately half of the extreme wind profiles does not overlap with shear and veer: for strong winds and stable conditions, the buoyancy force acts to maintain the stratification, whereas under unstable conditions the shear-induced turbulence is only reinforced by buoyancy forces, leading to well-mixed boundary layers without much shear or veer in the mixed layer. The median of  $Ri_B$  is 0.017 for all extreme wind speeds, but 0.028 for extreme winds that coincide with extreme shear.

In a similar manner we found that LLJs and extreme winds never coincide, but wind ramps are sometimes associated with LLJs and sometimes with extreme wind speeds (not shown). Little overlap between  $\sigma_u$  and turbulence intensity appears, as noted before. While the former often coincides with extreme wind speeds, neither of these proxies overlap with extreme shear profiles. Again, this can be explained by the fact that extreme shear is mostly observed under stable conditions, where buoyancy acts to suppress turbulent mixing. The fact that both turbulence proxies give the same result in this case, supports that under stably stratified conditions, even under relatively strong wind shear, turbulence is weak.

## 5. Discussion

We have found that low-level jets occur up to 12% of the time at the North Sea, exactly in the rotor plane of current-day wind turbines. Traditional wind profile parametrizations, such as the logarithmic wind profile and the power law approach, are unsuitable to describe these wind profiles and therefore a reference climatology such as illustrated in (Fig. 1) is incomplete and biased. Instead, one must separately account for LLJs, and these records should be removed from the dataset before deriving wind speed distribution parameters that can be used in conjunction with profile parametrizations.

Our findings suggest that the formation of LLJs is most frequent under stable stratification in spring and when the wind is directed offshore, similarly as found over the Baltic Sea (Dörenkämper et al., 2015). It would be worthwhile to evaluate their representation in mesoscale models, to assess the spatial characteristics and physical mechanisms governing these jets and their relation to low-level jets that formed onshore.

Stability also plays a key role in distinguishing between extreme wind speed profiles and extreme shear profiles. The strongest wind speeds typically occur in winter, when the sea is relatively warm with respect to the overlying or advected air. This leads to unstable stratification, where buoyancy forces act to enhance turbulent mixing, ultimately resulting in well-mixed profiles. In contrast, one finds the highest wind shear under stable conditions, when buoyancy suppresses turbulent mixing.

Traditionally, shear is thought to be a turbulence-producing process; e.g. Moeng and Sullivan (1994) systematically studied the differences between buoyancy- and shear-driven boundary layers for

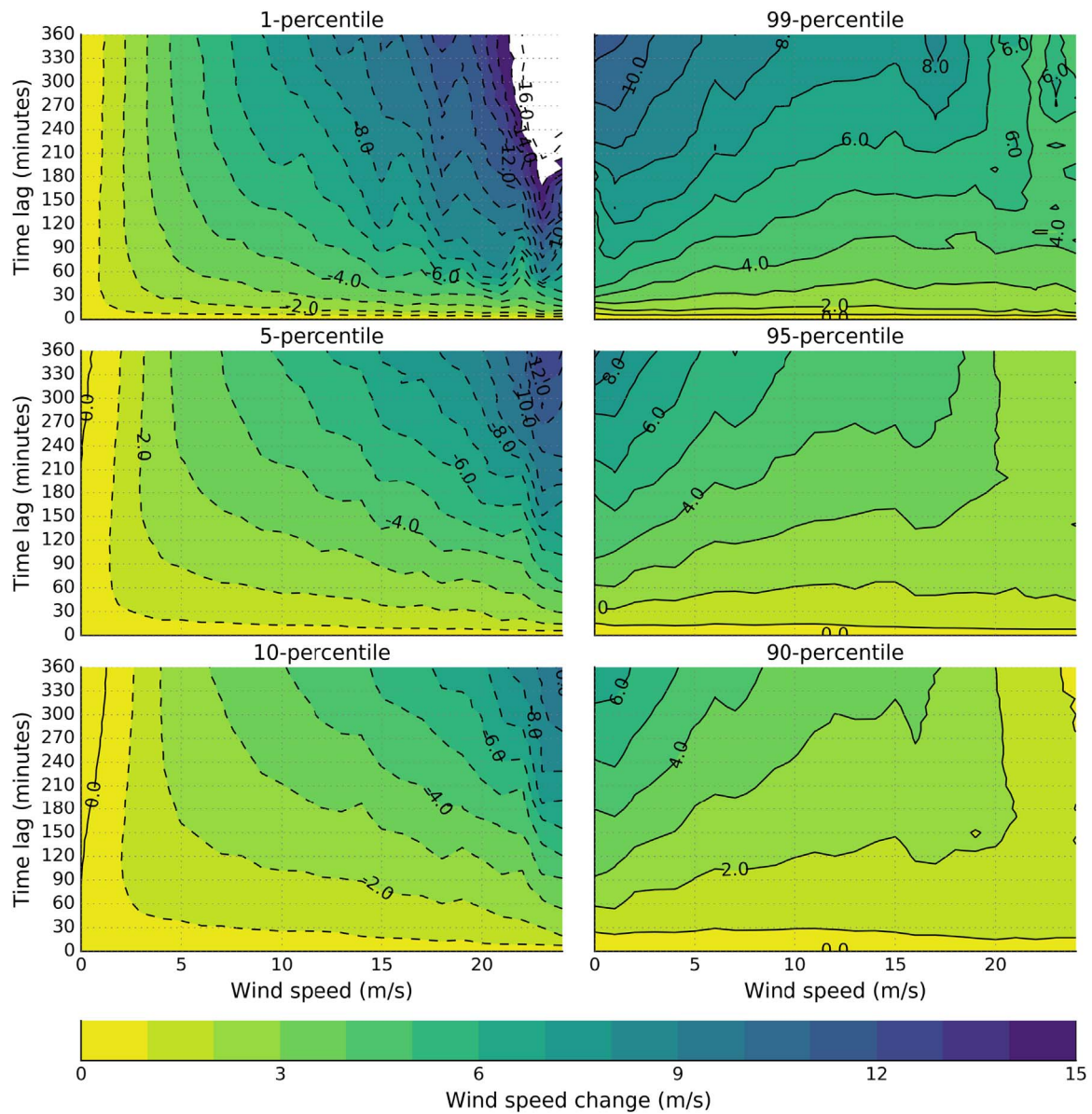


**Fig. 7.** Expected wind speed ramp event with given probability (plot title), given a wind speed and time lag. Dashed contours indicate negative values; the colorbar shows ramp magnitude only.

unstable conditions, and found strong wind streaks in the shear-driven boundary layer, together with a high vertical momentum flux ( $\overline{u'w'}$ ). Our results suggest that offshore, stratification is the dominant mechanism for the manifestation of shear, rather than vice versa. We therefore suggest that more systematic modelling studies are conducted to further understand this subtle balance.

We found that different proxies for turbulence intensity lead to different climatologies, illustrating that more detailed, higher frequency data is essential for an accurate description and classification of turbulence. Our analysis was limited by the instrumentation of the mast and the 10-min intervals at which the data were available. Observations closer to the surface and flux data from sonic anemometers would greatly enhance the possibilities to relate this dataset to other datasets as well as to evaluate it with classical boundary layer theory. For future studies it is imperative that measurements are taken closer to the surface, and include typical boundary layer parameters such as shear stress and higher-order moments.

We have assessed the sensitivity of the climatology to the thresholds used. For low-level jets, the sensitivity was reported to be within 2–3%. If,

for the other AWEs, the 93- or 97-percentiles are used rather than the 95-percentile, the absolute quantile values may show non-negligible differences, but the patterns that were discovered in the external conditions remain nearly identical. This small sensitivity underlines the robustness of the current findings.

Analyzing accumulated shear over different layers allowed us to include LLJs, which would not have been possible in traditional methods that would quantify shear as the ratio of wind speeds at two heights, or with a power law. By treating the occurrence of anomalous events in a boolean framework we were able to present a novel and consistent climatology of anomalous wind events.

Finally, it is worthwhile to consider the impact of anomalous wind events on turbine loads and power production. Low-level jets, normal (directional) wind shear, and wind ramps are not considered in the contemporary load assessment guidelines. Extreme wind speed and turbulence are considered, but in a very artificial manner. The way in which we treated these anomalous wind events fits very well with the load assessment procedure: there are load cases for normal conditions and load cases for the extremes. It would be very informative to set up

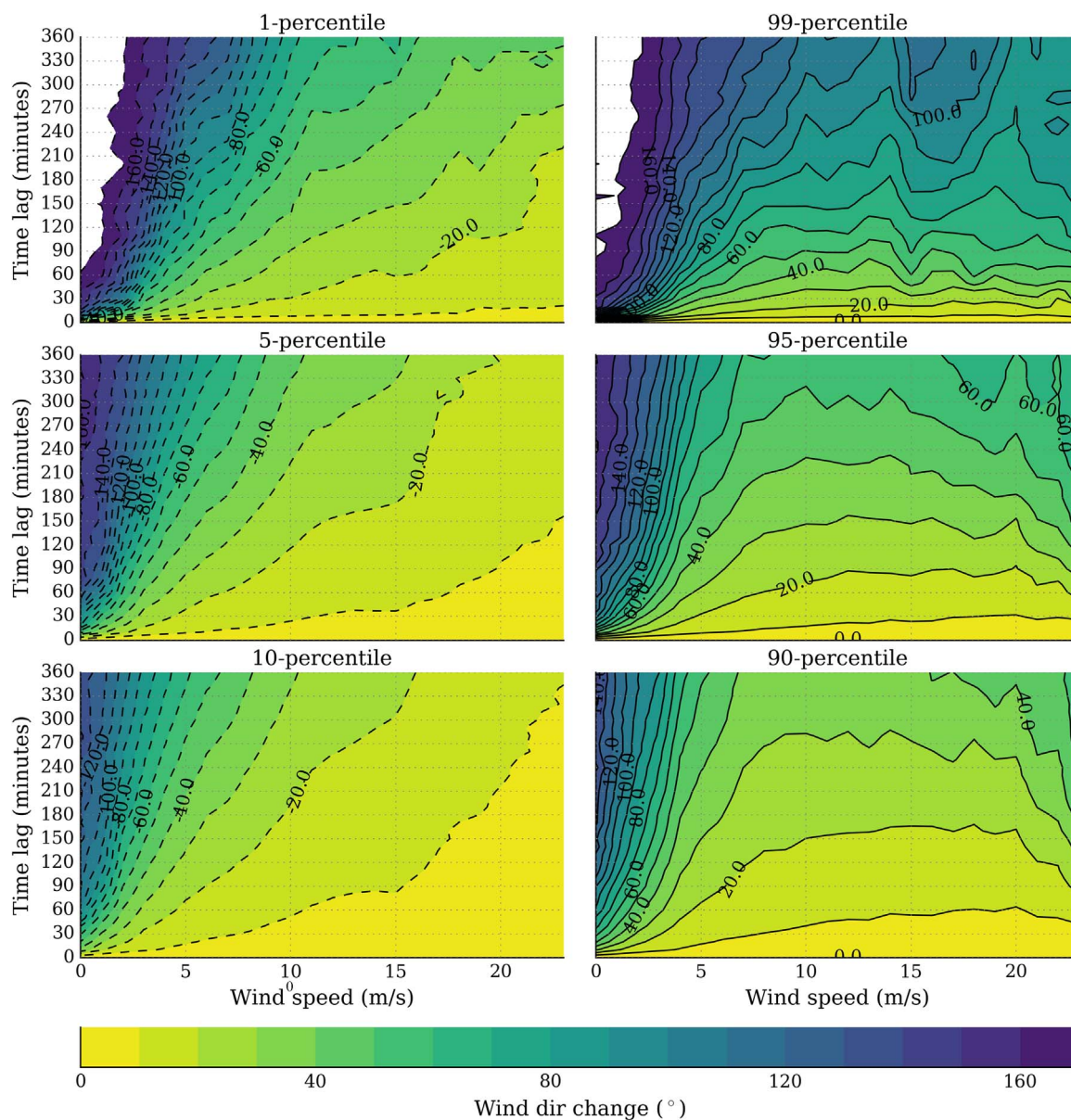


Fig. 8. Expected wind direction ramp event with given probability (plot title), given a wind speed and time lag. Dashed contours indicate negative values; the colorbar shows ramp magnitude only.

additional load cases for low-level jets, wind profiles with directional shear and load cases with transient mean wind profiles (wind ramps). Our observational study can be used as a basis for these load cases, but an approach in which meteorological models are coupled to the load assessment procedure is even better. A proof of concept on this methodology has already been published by Park et al. (2014).

### 6. Conclusions

We have analyzed observations up to 300 m from the IJmuiden metemast, situated in the North Sea 85 km off the Dutch coast. Six types of ‘anomalous wind events’ (AWEs) were defined to characterize certain extremes in the wind climate: low-level jets, extreme shear, both in wind speed and direction, extreme turbulence and gusts, and wind ramps (sudden transitions). This list covers the most important phenomena for wind industry, but it is certainly not exhaustive. Other AWEs can be defined and analyzed following a similar methodology.

Our first objective was to objectively define the anomalous wind events, and to describe them in terms of typical values. We found that 4.6% of the profiles should be classified as low-level jets, but with a distinct seasonal variability (up to 12% in July) related to SST. The 50-year wind extreme at hub height was found to be  $42.7 \pm 2.4 \text{ m s}^{-1}$ . For the classification of wind ramps we introduced several new figures that provide a comprehensive overview of wind ramps on different time scales and for different wind regimes.

To assess the temporal variability of anomalous wind events as well as their relation to other weather conditions, we took the values that are exceeded exactly 5% of the time. We found different weather regimes that are favourable for the formation of AWEs. This provided clues as to the underlying mechanisms, but in-depth case studies will be required to draw solid conclusions. Stability seems to play a very important role in the manifestation of several AWEs. Overlap between the various AWEs was assessed with the use of Venn diagrams. Although some extremes coincide, most AWEs are independent of each other.

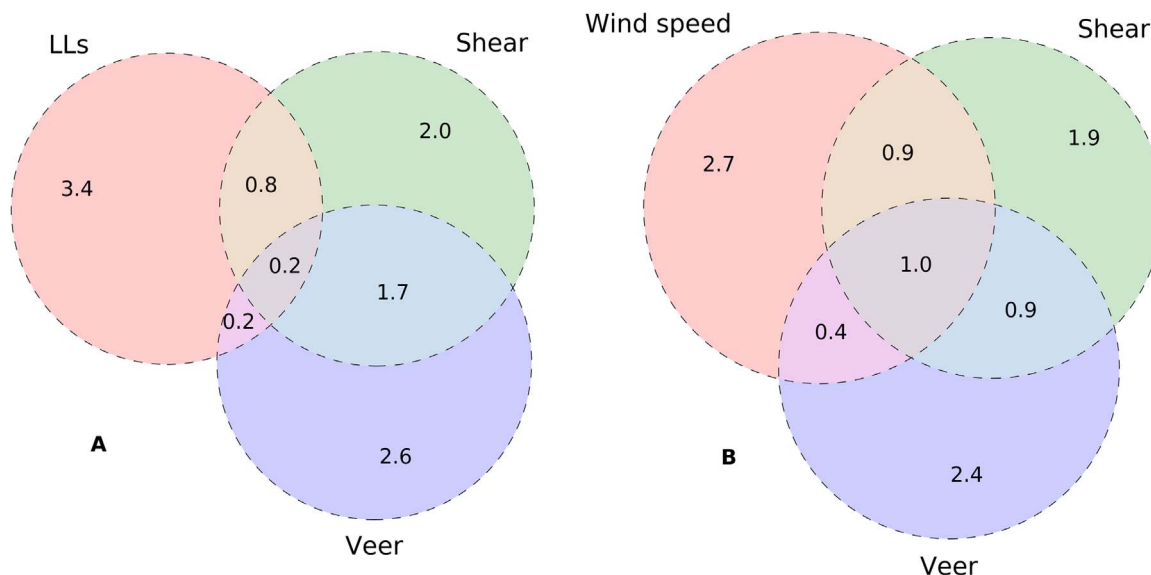


**Fig. 9.** Venn diagram of related anomalous wind events. A: Low-level jets, extreme shear profiles and extreme veer profiles. B: Extreme wind speeds, extreme shear and extreme veer profiles. Numbers are in percent of total data.

This reference climatology will act as the point of departure for case studies with meteorological models to enhance mechanistic understanding of the presented AWEs.

### Acknowledgements

This research is supported by the Dutch Technology Foundation STW, which is part of the Netherlands Organisation for Scientific Research (NWO), and which is partly funded by the Ministry of Economic Affairs (STW project number: 14185). Personal communication with Wim Bierbooms, Maarten Holtslag and Lidewij van den Brink shed light on various offshore wind topics.

### References

- Andreas, E.L., Claffy, K.J., Makshtas, A.P., 2000. Low-level atmospheric jets and inversions over the Western Weddell Sea. *Bound.-Layer Meteorol.* 97 (3), 459–486.
- Baas, P., Bosveld, F.C., Klein Baltink, H., Holtslag, A.A.M., 2009. A climatology of nocturnal low-level jets at Cabauw. *J. Appl. Meteor. Climatol.* 48 (8), 1627–1642.
- Bardal, L.M., Sætran, L.R., 2016. Wind gust factors in a coastal wind climate. *Energy Procedia* 94, 417–424.
- Breton, S.-P., Moe, G., 2009. Status, plans and technologies for offshore wind turbines in Europe and North America. *Renew. Energy* 34 (3), 646–654.
- Brown, A.R., Beljaars, A.C.M., Hersbach, H., Hollingsworth, A., Miller, M., Vasiljevic, D., 2005. Wind turning across the marine atmospheric boundary layer. *Q. J. R. Meteorol. Soc.* 131 (607), 1233–1250.
- Burk, S.D., Thompson, W.T., 1996. The summertime low-level jet and marine boundary layer structure along the California Coast. *Mon. Wea. Rev.* 124 (4), 668–686.
- Burton, T., Jenkins, N., Sharpe, D., Bossanyi, E., 2011. *Wind Energy Handbook* Second edition. John Wiley & Sons, Ltd., Chichester, UK.
- Carroll, J., McDonald, A., Dinwoodie, I., McMillan, D., Revie, M., Lazakis, I., 2017. Availability, operation and maintenance costs of offshore wind turbines with different drive train configurations. *Wind Energy*, (in press).
- Christakos, K., Cheliotis, I., Varlas, G., Steeneveld, G.-J., 2016. Offshore wind energy analysis of cyclone Xaver over North Europe. *Energy Procedia* 94, 37–44.
- Coelingh, J.P., van Wijk, A.J.M., Cleijne, J.W., Pleune, R., 1992. Description of the North Sea wind climate for wind energy applications. *J. Wind Eng. Ind. Aerodyn.* 39 (1), 221–232.
- Coelingh, J.P., van Wijk, A.J.M., Holtslag, A.A.M., 1996. Analysis of wind speed observations over the North Sea. *J. Wind Eng. Ind. Aerodyn.* 61 (1), 51–69.
- Cook, N.J.N.J., 1985. *The designer's guide to wind loading of building structures / Pt.1., Butterworths, UK.*
- Desmond, C., Murphy, J., Blonk, L., Haans, W., 2016. Description of an 8 MW reference wind turbine. *J. Phys.:Conf. Ser.* 753 (9), 092013.
- Donkers, J.A.J., Brand, A.J., Eecen, P.J., 2011. *Offshore Wind Atlas of the Dutch part of the North Sea.* Presented at the EWEA 2011, Brussels, Belgium, 14–17 March 2011 (<https://www.ecn.nl/docs/library/report/2011/m11031.pdf>).
- Dörenkämper, M., Optis, M., Monahan, A., Steinfeld, G., 2015. On the offshore advection of boundary-layer structures and the influence on offshore wind conditions. *Bound.-Layer Meteorol.* 155 (3), 459–482.
- Dotzek, N., Emeis, S., Lefebrvre, C., Gerpott, J., 2010. Waterspouts over the North and Baltic Seas: observations and climatology, prediction and reporting. *Meteorol. Z.* 19 (1), 115–129.
- European Wind Energy Association, 2013. *Where's the money coming from? Financing offshore wind farms, November 2013, isbn: 978-2-930670-06-5, URL: (http://www.ewea.org/fileadmin/files/library/publications/reports/Financing\_Offshore\_Wind\_Farms.pdf).*
- Fairall, C.W., Bradley, E.F., Hare, J.E., Grachev, A.A., Edson, J.B., 2003. Bulk parameterization of air-sea fluxes: updates and verification for the COARE Algorithm. *J. Clim.* 16 (4), 571–591.
- Farrugia, R.N., 2003. The wind shear exponent in a Mediterranean island climate. *Renew. Energy* 28 (4), 647–653.
- Foken, T., 2006. 50 Years of the Monin-Obukhov Similarity Theory. *Bound.-Layer Meteorol.* 119 (3), 431–447.
- Gallego, C., Cuerva, I., Costa, A., 2014. Detecting and characterising ramp events in wind power time series. *J. Phys.:Conf. Ser.* 555 (1), 012040.
- Gallego-Castillo, C., Cuerva-Tejero, A., Lopez-Garcia, O., 2015. A review on the recent history of wind power ramp forecasting. *Renew. Sustain. Energy Rev.* 52, 1148–1157.
- Garratt, J.R., 1977. Review of Drag Coefficients over Oceans and Continents. *Mon. Wea. Rev.* 105 (7), 915–929.
- Gryning, S.-E., Batchvarova, E., Brümmner, B., Jørgensen, H., Larsen, S., 2007. On the extension of the wind profile over homogeneous terrain beyond the surface boundary layer. *Bound.-Layer Meteorol.* 124 (2), 251–268.
- Gutierrez, W., Araya, G., Kiliyanpilakkil, P., Ruiz-Columbie, A., Tutkun, M., Castillo, L., 2016. Structural impact assessment of low level jets over wind turbines. *J. Renew. Sustain. Energy* 8, 2.
- Hansen, K.S., Barthelmie, R.J., Jensen, L.E., Sommer, A., 2012. The impact of turbulence intensity and atmospheric stability on power deficits due to wind turbine wakes at Horns Rev wind farm. *Wind Energy* 15 (1), 183–196.
- Harris, R.I., 1999. Improvements to the 'Method of Independent Storms'. *J. Wind Eng. Ind. Aerodyn.* 80 (1–2), 1–30.
- Hollingsworth, A., 1994. Validation and diagnosis of atmospheric models. *Dyn. Atmos. Oceans* 20 (3), 227–246.
- Holtslag, A.A.M., 1984. Estimates of diabatic wind speed profiles from near-surface weather observations. *Bound.-Layer Meteorol.* 29 (3), 225–250.
- Holtslag, M.C., Bierbooms, W.a.a.M., Bussel, G.J.W., 2016. Wind turbine fatigue loads as a function of atmospheric conditions offshore. *Wind Energy* 19 (10), 1917–1932.
- Holtslag, M.C., Bierbooms, W.A.A.M., van Bussel, G.J.W., 2015. Validation of surface layer similarity theory to describe far offshore marine conditions in the Dutch North Sea in scope of wind energy research. *J. Wind Eng. Ind. Aerodyn.* 136, 180–191.
- IEC, 2005. *IEC 61400-1: Wind turbines - Part 1: Design requirements.*
- IEC, 2009. *IEC 61400-3: Wind turbines - Part 3: Design requirements for offshore wind turbines.*
- Irwin, J.S., 1979. A theoretical variation of the wind profile power-law exponent as a function of surface roughness and stability. *Atmos. Environ.* (1967) 13 (1), 191–194.
- Kettle, A.J., 2014. Unexpected vertical wind speed profiles in the boundary layer over the southern North Sea. *J. Wind Eng. Ind. Aerodyn.* 134, 149–162.
- Kiviluoma, J., Holttinen, H., Weir, D., Scharff, R., Söder, L., Menemenlis, N., Cutululis, N.A., Danti Lopez, I., Lannoye, E., Estanqueiro, A., Gomez-Lazaro, E., Zhang, Q., Bai, J., Wan, Y.-H., Milligan, M., 2016. Variability in large-scale wind power generation. *Wind Energy* 19 (9), 1649–1665.
- Kuik, G.A.M.v., Peinke, J., Nijssen, R., Lekou, D., Mann, J., Sørensen, J.N., Ferreira, C., van Wingerden, J.W., Schlipf, D., Gebraad, P., Polinder, H., Abrahamson, A., van Bussel, G.J.W., Sørensen, J.D., Tavner, P., Bottasso, C.L., Muskulus, M., Matha, D.,

- Lindeboom, H.J., Degraer, S., Kramer, O., Lehnhoff, S., Sonnenschein, M., Sørensen, P.E., Künnike, R.W., Morthorst, P.E., Skytte, K., 2016. Long-term research challenges in wind energy – a research agenda by the European Academy of Wind Energy. *Wind Energy Sci.* 1 (1), 1–39.
- Lamb, H., Frydendahl, K., 1991. *Historic Storms of the North Sea, British Isles and Northwest Europe*. Cambridge University Press.
- Lange, B., Larsen, S., Højstrup, J., Barthelmie, R., 2004. Importance of thermal effects and sea surface roughness for offshore wind resource assessment. *J. Wind Eng. Ind. Aerodyn.* 92 (11), 959–988.
- Martini, M., Guanche, R., Losada, I.J., Vidal, C., 2017. Accessibility assessment for operation and maintenance of offshore wind farms in the North Sea. *Wind Energy* 20 (4), 637–656.
- Maureira Poveda, J.P., Wouters, D., 2014. *Wind Measurements at Meteorological Mast IJmuiden*. Technical Report ECN-E-14-058, ECN, Petten.
- Méridaud, A., Ringwood, J.V., 2016. Condition-based maintenance methods for marine renewable energy. *Renew. Sustain. Energy Rev.* 66, 53–78.
- Mirocha, J.D., Simpson, M.D., Fast, J.D., Berg, L.K., Baskett, R.L., 2016. Investigation of boundary-layer wind predictions during nocturnal low-level jet events using the Weather Research and Forecasting model. *Wind Energy* 19 (4), 739–762.
- Moeng, C.-H., Sullivan, P.P., 1994. A Comparison of Shear- and Buoyancy-Driven Planetary Boundary Layer Flows. *J. Atmos. Sci.* 51 (7), 999–1022.
- Nunalee, C.G., Basu, S., 2014. Mesoscale modeling of coastal low-level jets: implications for offshore wind resource estimation. *Wind Energy* 17 (8), 1199–1216.
- Oost, W.A., Komen, G.J., Jacobs, C.M.J., van Oort, C., Bonekamp, H., 2001. Indications for a wave dependent charnock parameter from measurements during ASGAMAGE. *Geophys. Res. Lett.* 28 (14), 2795–2797.
- Optis, M., Monahan, A., Bosveld, F.C., 2014. Moving Beyond Monin-Obukhov Similarity Theory in Modelling Wind-Speed Profiles in the Lower Atmospheric Boundary Layer under Stable Stratification. *Bound.-Layer Meteorol.* 153 (3), 497–514.
- Palutikof, J.P., Brabson, B.B., Lister, D.H., Adcock, S.T., 1999. A review of methods to calculate extreme wind speeds. *Met. Appl.* 6 (2), 119–132.
- Park, J., Basu, S., Manuel, L., 2014. Large-eddy simulation of stable boundary layer turbulence and estimation of associated wind turbine loads. *Wind Energy* 17 (3), 359–384.
- Peña, A., Floors, R., Sathe, A., Gryning, S.-E., Wagner, R., Courtney, M.S., Larsen, X.G., Hahmann, A.N., Hasager, C.B., 2015. Ten years of boundary-layer and wind-power meteorology at Høvsøre, Denmark. *Bound.-Layer Meteorol.* 158 (1), 1–26.
- Peña, A., Hasager, C.B., Gryning, S.-E., Courtney, M., Antoniou, I., Mikkelsen, T., 2009. Offshore wind profiling using light detection and ranging measurements. *Wind Energy* 12 (2), 105–124.
- REN21, 2016. *Renewables 2016 Global Status Report (Paris: REN21 Secretariat)*, (<http://www.ren21.net/GSR-2016-Report-Full-report-EN>).
- Rodrigues, S., Restrepo, C., Kontos, E., Teixeira Pinto, R., Bauer, P., 2015. Trends of offshore wind projects. *Renew. Sustain. Energy Rev.* 49, 1114–1135.
- Skamarock, W.C., Klemp, J.B., 2008. A time-split nonhydrostatic atmospheric model for weather research and forecasting applications. *J. Comput. Phys.* 227 (7), 3465–3485.
- Smedman, A.-S., Tjernström, M., Högström, U., 1989. Analysis of the turbulence structure of a marine low-level jet. *Bound.-Layer Meteorol.* 66 (1–2), 105–126.
- Smith, S.D., 1988. Coefficients for sea surface wind stress, heat flux, and wind profiles as a function of wind speed and temperature. *J. Geophys. Res.* 93 (C12), 15467–15472.
- Stensrud, D.J., 1996. Importance of low-level jets to climate: a review. *J. Clim.* 9 (8), 1698–1711.
- Storm, B., Basu, S., 2010. The WRF Model Forecast-Derived Low-Level Wind Shear Climatology over the United States Great Plains. *Energies* 3 (2), 258–276.
- Stull, R.B., 1988. *An Introduction to Boundary Layer Meteorology*. Springer, Dordrecht, Netherlands.
- AWS Truewind, 2008. *AWS Truewind's final report for the Alberta forecasting pilot project*. Tech. rep. (available at ([http://www.uwig.org/Alberta\\_PP\\_Final\\_Report\\_AWST\\_Jun25.pdf](http://www.uwig.org/Alberta_PP_Final_Report_AWST_Jun25.pdf))).
- Van de Wiel, B.J.H., Moene, A.F., Steeneveld, G.J., Baas, P., Bosveld, F.C., Holtslag, A.A.M., 2010. A conceptual view on Inertial Oscillations and Nocturnal Low-Level Jets. *J. Atmos. Sci.* 67 (8), 2679–2689.
- Van Ulden, A.P., Holtslag, A.A.M., 1985. Estimation of atmospheric boundary layer parameters for diffusion applications. *J. Clim. Appl. Meteorol.* 24 (11), 1196–1207.
- Van Wijk, A.J.M., Beljaars, A.C.M., Holtslag, A.A.M., Turkenburg, W.C., 1990. Evaluation of stability corrections in wind speed profiles over the North Sea. *J. Wind Eng. Ind. Aerodyn.* 33 (3), 551–566.
- Vorpahl, F., Schwarze, H., Fischer, T., Seidel, M., Jonkman, J., 2013. Offshore wind turbine environment, loads, simulation, and design. *WENE* 2 (5), 548–570.
- Wallace, J.M., Hobbs, P.V., 2006. *Atmospheric Science: An Introductory Survey*. Academic Press. ISBN: 978-0-12-732951-2.
- Werkhoven, Verhoef, H., 2012. *Offshore Meteorological Mast IJmuiden - Abstract of Instrumentation Report*. Technical report, URL: ([http://www.meteomastijmuiden.nl/fileadmin/meteomastijmuiden/ECN-Wind\\_Memo-12-010\\_Abtract\\_of\\_Instrumentatierapport\\_Meetmast\\_IJmuiden.pdf](http://www.meteomastijmuiden.nl/fileadmin/meteomastijmuiden/ECN-Wind_Memo-12-010_Abtract_of_Instrumentatierapport_Meetmast_IJmuiden.pdf)).
- Westerhellweg, Annette, Beatriz Canadillas, Thomas Neumann. *Direction dependency of offshore turbulence intensity in the German Bight*, DEWEK 2010 10th German wind energy conference, 2010.
- Wieringa, J., 1973. Gust factors over open water and built-up country. *Bound.-Layer Meteorol.* 3 (4), 424–441.
- Zack, J., 2007. Optimization of wind power production forecast performance during critical periods for grid management. *Wind Power 2007*, Los Angeles, URL: ([https://www.awstruepower.com/assets/AWEA\\_Windpower\\_2007\\_Forecasting.pdf](https://www.awstruepower.com/assets/AWEA_Windpower_2007_Forecasting.pdf)).
- Zemba, J., Friehe, C.A., 1987. The marine atmospheric boundary layer jet in the Coastal Ocean Dynamics Experiment. *J. Geophys. Res.* 92 (C2), 1489–1496.